Heliyon 10 (2024) e35203

Contents lists available at ScienceDirect

Heliyon

journal homepage: www.cell.com/heliyon

Research article

Comparison of single-shot, FOCUS single-shot, MUSE, and FOCUS MUSE diffusion weighted imaging for pulmonary lesions: A pilot study

Jie Li [a,b,1], Yi Xia [b,1], JianKun Dai [c,1], GuangYuan Sun [d,1], MeiLing Xu [b], XiaoQing Lin [a,b], LingLing Gu [b], Jie Shi [c], ShiYuan Liu [b], Li Fan [b,*]

[a] College of Health Sciences and Engineering, University of Shanghai for Science and Technology, No.516 Jungong Road, Shanghai, 200093, China
[b] Department of Radiology, Second Affiliated Hospital of Naval Medical University, No. 415 Fengyang Road, Shanghai, 200003, China
[c] GE Healthcare, Beijing, 100000, China
[d] Department of Thoracic Surgery, Second Affiliated Hospital of Naval Medical University, No. 415 Fengyang Road, Shanghai, 200003, China

ARTICLE INFO

Keywords:
Magnetic resonance imaging
Diffusion weighted imaging
Lung
Pulmonary lesions

ABSTRACT

Rationale and objectives: To compare the performance of SS, FOCUS SS, MUSE, and FOCUS MUSE DWI for pulmonary lesions to obtain a better technique for pulmonary DWI imaging.

Materials and methods: 44 patients with pulmonary lesions were recruited to perform pulmonary DWI using SS, FOCUS SS, MUSE, and FOCUS MUSE sequences. Then, two radiologists with 12 and 10 years of chest MRI experiences assessed the overall image quality while another two radiologists both with 3 years of experiences evaluated the SNR, DR, and ADC of pulmonary lesions. Using interclass correlation coefficient (ICC) and kappa statistics to assess consistency of readers, Friedman test and Dunn-Bonferroni post hoc were used to calculate the difference between sequences. Mann-Whitney test and ROC curve were used to distinguish malignant from benign lesions.

Results: All the assessed variables of the four sequences presented good to excellent intra-/inter-observer consistency. Compared with SS, FOCUS SS and MUSE, FOCUS MUSE demonstrated better image quality, including significantly higher 5-point Likert scale score ($P < 0.001$) and smaller DR ($P < 0.001$). SNR was comparable among SS, FOCUS SS, and FOCUS MUSE ($P > 0.05$) while MUSE presented with significantly higher SNR over them ($P < 0.01$). ADC of malignant was significantly smaller than that of benign for all the four sequences ($P < 0.05$). ROC analysis showed relatively better diagnostic performance of FOCUS MUSE (AUC = 0.820) over SS (AUC = 0.748), FOCUS SS (AUC = 0.778), and MUSE (AUC = 0.729) in distinguishing malignant from benign lesions.

Conclusion: FOCUS MUSE possessed sufficient SNR and was better over SS, FOUCS SS, and MUSE for characterizing pulmonary lesions.

* Corresponding author.
E-mail address: fanli0930@163.com (L. Fan).
[1] These authors contributed equally to this work.

https://doi.org/10.1016/j.heliyon.2024.e35203
Received 26 October 2023; Received in revised form 23 July 2024; Accepted 24 July 2024
Available online 25 July 2024

1. Introduction

According to the latest global cancer statistics, lung cancer remained the leading cause of cancer-related death worldwide, accounting for 1.8 million deaths in 2020 [1]. Thus, it would have clinical significance to detect pulmonary lesions, distinguish malignant from benign lesions for guiding treatment decisions selection, and predict prognosis [2]. Currently, despite of ionizing radiation, computed tomography (CT) remains the primary tool for the diagnosis of pulmonary lesions. Magnetic resonance imaging (MRI) is a non-invasive and free of ionizing radiation technique routinely used for disease examination. But the application of MRI in lung is behindhand compared with other organs mainly due to the lung's low proton density, substantial magnetic susceptibility artifacts caused by multiple air-tissue interfaces, and the influence of cardiac and respiratory motions [3]. Nevertheless, with the development of hardware, imaging and reconstruction techniques, MRI has shown the capability of providing morphological, functional, and metabolic information of pulmonary lesions. Based on fruitful research results, the Fleischner Society has recommended the use of MRI for lung diseases, such as pulmonary nodule detection and lung cancer staging [4].

Diffusion-weighted imaging (DWI) is an advanced MRI technique which can reveal tissue microstructure, such as cellularity and extracellular space size, by probing the motion process of water molecules [5]. It is a fundamental sequence in oncologic imaging and has emerging applications in the chest [6]. Previous studies had reported a variety of DWI applications of lung including distinguishing malignant from benign lesions [5,7,8], differentiation of tumor subtypes [9], tumor staging [10], evaluating mediastinal lymph node metastasis [11], predicting treatment response [12] and prognosis [13], reflecting tumor Ki-67 expression level [14], and characterizing tumor cellularity [15]. Now, DWI has become part of state-of-the-art multiparametric MRI protocols for assessment of the chest [6].

Single-shot echo-planar imaging (SS-EPI) is a widely used technique to acquire clinical DWI because of its fast imaging and decreased motion artifact properties [16]. However, SS-EPI is sensitive to main magnetic field inhomogeneities and highly prone to geometric distortions along the phase-encoding direction [16]. SS-EPI based DWI is particularly challenge for lung as an organ with substantial air-tissue interfaces. The distortion of DWI may have an impact on tumor delineation, tumor characterization and response assessment. Besson et al. [17], corrected the distortion by image post-processing using the information from additionally scanned DWI with reversed phase-encoding polarity, and found significant improved space coregistration with PET images for all lung tumors. There are a few studies using fast spin echo (FSE) based DWI to reduce susceptibility induced pulmonary lesion distortion [9,18–20] at the expense of longer scan time and lower SNR than SS-EPI DWI [18–20]. The application of improved EPI based DWI techniques may be another way to reduce the susceptibility artifacts while maintain sufficient SNR.

Field-of-view optimization (FOV) and constrained undistorted single shot (FOCUS) is a technique that applies a two-dimensional spatially selective echo-planar radiofrequency excitation pulse and a 180° refocusing pulse to reduce the FOV in the phase-encoding direction [21]. This method allows decreasing the required readout duration for SS-EPI resulting with better DWI images [21]. Previous studies have shown the capability of FOCUS SS-EPI DWI to decrease image distortions and provide better anatomic details in thyroid gland [22], nasopharynx [23], pancreas [24], breast [25], rectum [26] and columna vertebralis [27]. Multiplexed sensitivity-encoding (MUSE) is a technique inherently estimating both linear and nonlinear phase variations from multi-shot segmented EPI DWI data with aim of achieving better spatial resolution and high signal-to-noise ratio (SNR), and alleviating distortions [28]. Previous studies have reported that, compared with SS-EPI, MUSE is able to minimize image deformation and provide better image quality for brain [29], rectum [30], breast [31],cervix [32] and liver [33]. FOCUS can also be integrated with MUSE which may further improve the DWI image quality. Recently, Bai et al. [34], had firstly investigated the performance of FOCUS MUSE for pancreas, showing the advantages of FOCUS MUSE over SS, FOCUS SS and MUSE, including the best image quality and most stable apparent diffusion coefficient (ADC) measurement.

Despite DWI has emerging applications in the lung, it remains unknown if the improved EPI based DWI techniques could be beneficial for lung lesion evaluation. Thus, the aim of this pilot study was to compare the performance of FOCUS SS, MUSE, and FOCUS MUSE with routinely used SS-EPI DWI for lung lesions. The 5-point Likert scale score of overall image quality, and the SNR, distortion ratio (DR), and ADC of lesions were estimated and compared among the four sequences, separately. The capability of ADC for distinguishing malignant from benign lesions were also compared among the four sequences.

2. Materials and Methods

2.1. Patients

This pilot study was approved by the institutional review board and the ethics committee (2023SL028). All the participants signed informed consent and accepted MRI examinations.

Inclusion criteria: people with previous chest CT suggestive of at least one lung nodule with maximum lesion greater than 5 mm, people at high risk of lung cancer (e.g., aged 50–80 years old with a long history of smoking or long-term exposure to carcinogens, people with a family history of lung cancer, and people with chronic obstructive pulmonary disease). Exclusion criteria: 1) those with contraindications to MRI; 2) history of thoracic surgery; 3) patients with neurological disorders such as central respiratory injury that prevent normal inspiration and breath-holding; 4) patients with coughing, breathlessness that prevents normal inspiration and breath-holding; 5) other conditions that the clinical staffs consider inappropriate for this test. The criteria for midway roll-out are based on the patient's voluntary midway withdrawal.

According to the inclusion and exclusion criteria, a total of 48 patients with lung lesions was recruited from November 2022 to May 2023. All of them underwent MRI before treatment, biopsy, and surgery. The DWI images of four patients were excluded for analysis

due to severe motion artifacts. The remain 44 patients were used for subjective overall image quality score. One patient was not used to estimate the SNR, DR, and ADC because the lesion was not clearly depicted in all the four DWI images.

2.2. MRI acquisition

All patients were scanned using 3.0T MRI (Signa Premier; GE Healthcare, Milwaukee, USA) in supine position using a 21-channel multipurpose coil. Axial PROPELLER T2-weighted imaging (T2WI) and DWIs (including SS, FOCUS SS, MUSE, and FOCUS MUSE) of lung were acquired with respiratory triggered. The imaging parameters were summarized in Table 1.

2.3. Image analysis

All assessments were performed on the workstation (AW4.7; GE Healthcare, Milwaukee, USA). Image analysis was carried out independently by four radiologists (Y.X., L.G., J.L. and X.L.) with 12, 10, 3 and 3 years of thoracic MRI experience, respectively. All were blind to the patients' clinical information.

The overall image quality of DWIs (b value = 800 s/mm^2) was visually assessed by Y.X. and L.G. independently using 5-point Likert scale score [35]: 1 point, poor (heavy noise/artifacts, undetectable lesion, no anatomical detail of the lesion); 2 points, fair (noise/-artifacts are large and seriously affect the diagnosis of the lesion, poorly defined lesion margins, little anatomical detail of the lesion visible, less clinical utility); 3 points, moderate (noise/artifacts as being able to meet the requirements of clinical diagnosis, lesion margins intact, lesion anatomical details visible); 4 points, good (noise/artifacts are small and do not affect the imaging diagnosis, clear depiction of lesions, better anatomical detail of lesions); 5 points, excellent (minimal artifacts/noises, clear depiction of the lesion, clear display of anatomical details of the lesion).

The SNR and DR were used to objectively assess the image quality of DWIs for pulmonary lesions [18]. Regions-of-interest (ROIs) were drawn manually by the J.L. and X.L. separately. For lesions, a single freehand ROI was defined by tracing a line along the lesion margins and avoiding the necrosis, cystic, hemorrhage regions and magnetic susceptibility artifacts on the slice containing the largest lesion area (Fig. S1). The mean and standard derivation (SD) of DWI signal intensity (SI) within the lesion ROIs were extracted for further analysis. The average SD of DWI SI of three circular lung parenchyma regions was used for SNR calculation [18]. The three circular regions were located on the same section as lesion and kept away from blood vessels, airways, and lesions.

The SNR was defined as the ratio between the mean SI of lesion (SI_{lesion}) and SD of lung parenchyma ($SD_{parenchyma}$) as given by:

$$SNR = SI_{lesion} / SD_{parenchyma} \quad [18]$$

DR was used to quantitatively estimate the image distortion level of DWI images with the anatomical T2WI as reference. The definition of DR was given by:

$$DR = A/B \quad [18]$$

A is the maximum lesion displacement in the phase-encoding direction between DWI and T2WI, and B is the lesion diameter in the phase-encoding direction on T2WI (Fig. S1).

The ADC map was fitted using the workstation. The mean ADC value of lesion was then extracted from the ADC map using the same lesion ROI for SNR.

After one month washout time, Y.X. re-assessed the overall image quality of DWIs (b value = 800 s/mm^2), and J.L. re-evaluated SNR, DR, and ADC of lesions.

Only one lesion with maximum diameter was used to evaluate SNR, DR, and ADC for each patient in this study.

Table 1
Scan parameters of the four DWI sequences and T2WI.

Sequence	SS	FOCUS SS	MUSE	FOCUS MUSE	T2WI
TR (ms)/TE (ms)	2222-6316/57.2	2222-6316/48.5	2222-6316/53.6	2222-6316/53.1	2400-5455/85
Field of view (cm^2)	40 × 40	32 × 16	36 × 36	32 × 16	42 × 42
Matrix size	168 × 168	132 × 68	148 × 148	132 × 68	300 × 300
In-plane resolution (mm^2)	2.4 × 2.4	2.4 × 2.4	2.4 × 2.4	2.4 × 2.4	1.4 × 1.4
Slice thickness (mm)	4	4	4	4	4
Number of slices	13	13	13	13	39
Number of shots	1	1	2	2	1
B factors(sec/mm^2)	0, 50, 800	0, 50, 800	0, 50, 800	0, 50, 800	/
Number of averages	1, 2, 6	1, 2, 6	1, 2, 6	1, 2, 6	1.5
Excitation mode	Selective	Focus	Selective	Focus	Selective
Acquisition time	1min26s-2min59s	1min10s-2min51s	2min21s-5min41s	2min34s-6min05s	2min21s-4min46s

SS = single-shot diffusion-weighted imaging; FOCUS = field of view optimized and constrained undistorted single-shot diffusion-weighted imaging; MUSE DWI = multiplexed sensitivity encoding diffusion-weighted imaging; FOCUS MUSE = field of view optimized and constrained undistorted multiplexed sensitivity encoding diffusion-weighted imaging.

2.4. Statistical analysis

Statistical analysis was performed using SPSS (version 27.0; IBM, NY, USA) and MedCalc (version 22.0; Mariakerke, Belgium). In this study, $P < 0.05$ was considered statistically significant.

The inter-observer and intra-observer variability for the overall image quality score was evaluated using kappa (κ) statistics. The inter-observer and intra-observer variability for the SNR, DR and ADC was assessed using the interclass correlation coefficient (ICC) test. Inter-observer and intra-observer consistency were also shown using Bland-Altman analysis. The κ and ICC values were interpreted as follows:0.00–0.20, poor agreement; 0.21–0.40, fair agreement; 0.41–0.60, moderate agreement; 0.61–0.80, good agreement; 0.81–1.00, excellent agreement [36]. The Friedman test was used to assess the differences of subjective score, SNR, DR, and ADC value among the four DWI sequences, and the Dunn-Bonferroni *post hoc* was used to adjust all paired comparisons with significantly difference. The Mann-Whitney was used to compare the ADC difference between benign and malignant pulmonary lesions. The receiver operating characteristic curve (ROC) was carried out and area under curve (AUC) was used to assess the performance of ADC value for discriminating malignant from benign lesions. The statistical power was calculated using the function "samplesizepwr" provided in Matlab (2021b; https://www.mathworks.com) for all two-sample comparison with $P < 0.05$.

3. Results

3.1. Patients characteristics

Four patients were excluded due to the DWI images suffered server motion artifacts. As a result, the final assessment was carried out using 44 patients (median age of 69 years; range 28–81 years), consisting of 29 males and 15 females. They all received histopathological examination after MRI in our hospital. Of those, 35 were histopathologically proven malignant pulmonary lesion with an average tumor size of 31.90 ± 14.87 mm (median, 33.11 mm; range, 6–78.5 mm). Most of the malignant (31/35) was non-small cell lung cancers (NSCLCs), including 18 adenocarcinomas, 11 squamous carcinomas and 2 nonidentified NSCLCs. The other malignant subtypes were consisted of small cell carcinomas (n = 2), adenosine squamous carcinoma (n = 1), and lymphoma (n = 1). Benign lesions (n = 9) had an average diameter of 23.70 ± 15.84 mm (median, 19.25 mm; range, 11.3–63.8 mm).

The DWIs of the finally included 44 patients were used for subjective overall image quality score. One adenocarcinoma patient with the lesion size of 8 mm was not used for quantitative analysis because the tumor can't be clearly shown in SS, FOCUS SS, and MUSE.

3.2. Inter-observer and intra-observer variability

For the subjective overall image quality assessed by 5-point Likert score, all the four DWI sequences demonstrated good to excellent intra-observer/inter-observer agreement with κ value of 0.854/0.677, 0.867/0.753, 0.830/0.744, and 0.771/0.801 for SS, FOCUS SS, MUSE, and FOCUS MUSE, respectively (Table 2).

The SNR and DR of lesion for SS, FOCUS SS, MUSE, and FOCUS MUSE also presented with good to excellent intra-observer/inter-observer agreement with the ICC value ranging from 0.766 to 0.870 and from 0.672 to 0.853, respectively (Table 2).

The intra-observer/inter-observer agreement of lesion ADC value was all excellent for SS, FOCUS SS, MUSE, and FOCUS MUSE with ICC of 0.954/0.943, 0.961/0.896, 0.974/0.949, and 0.964/0.922, respectively (Table 2).

The intra-observer (Fig. S2) as well as inter-observer (Fig. S3) difference of the above variables were also analyzed using Bland-Altman and most of the differences were almost filled within the 95 % interval. Taking the intra-observer/inter-observer agreement and Bland-Altman results into account, the overall image score assessed by Y.X. (twice) and L.G., as same as the SNR, DR, and ADC of lesion estimated by J.L. (twice) and X.L. was averaged, respectively, for following analysis in this study.

3.3. Comparisons of image quality and ADC

As shown in Table 3 and Fig. 1A, the average overall image score of FOCUS MUSE (4.58 ± 0.61) was significantly higher than that of SS (3.85 ± 0.65; $P < 0.001$), FOCUS SS (4.01 ± 0.70; $P < 0.001$), and MUSE (4.06 ± 0.66; $P < 0.001$). The FOCUS MUSE had median overall image score of 5 which was also significantly higher than that of SS (4; $P < 0.001$), FOCUS SS (4; $P < 0.001$), and MUSE (4; $P < 0.001$). No significant difference was observed for neither average nor median overall image score among SS, FOCUS SS, and MUSE ($P > 0.05$).

Table 3 and Fig. 1B showed the SNR of MUSE (72.23 ± 45.30) was significantly higher than that of SS (52.97 ± 30.97; $P < 0.001$), FOCUS SS (57.92 ± 33.84; $P = 0.002$), and FOCUS MUSE (52.26 ± 35.94; $P < 0.001$). There were no significant differences of SNRs among SS, FOCUS SS, and FOCUS MUSE ($P > 0.05$).

As demonstrated in Table 3 and Fig. 1C, FOCUS MUSE had the DR of 0.31 ± 0.22 which was significantly smaller than that of SS (0.68 ± 0.45; $P < 0.001$), FOCUS SS (0.57 ± 0.35; $P < 0.001$), and MUSE (0.60 ± 0.40; $P < 0.001$). No significant differences of DRs were found among SS, FOCUS SS and MUSE ($P > 0.05$).

The ADC value of lesion extracted from SS, FOCUS SS, MUSE, and FOCUS MUSE DWI was 1.39 ± 0.43 (10^{-3} mm^2/s), 1.38 ± 0.45 (10^{-3} mm^2/s), 1.44 ± 0.49 (10^{-3} mm^2/s), and 1.34 ± 0.46 (10^{-3} mm^2/s), respectively (Table 3). Friedman test didn't show significant difference of ADC among the four sequences (Table 3 and Fig. 1D; $P = 0.057$).

All statistical power of two-sample test with $P < 0.05$ for subjective score, SNR and DR were larger than 0.85, except that the statistical power of SNR comparison between FOCUS and MUSE was 0.73. MRI images from three representative patients were also

Table 2
Intra- and inter-observer concordance of subjective score, SNR, DR, and ADC for SS, FOCUS SS, MUSE, and FOCUS MUSE, respectively.

	Subjective score (κ)		SNR (ICC)		DR (ICC)		ADC (ICC)	
	Intra	Inter	Intra	Inter	Intra	Inter	Intra	Inter
SS	0.854(0.733–0.976)	0.677(0.495–0.858)	0.870(0.739–0.925)	0.831(0.522–0.858)	0.672(0.394–0.822)	0.673(0.386–0.816)	0.954(0.915–0.975)	0.943(0.896–0.969)
FOCUS SS	0.867(0.752–0.981)	0.753(0.596–0.910)	0.766(0.572–0.875)	0.849(0.681–0.906)	0.634(0.319–0.803)	0.744(0.496–0.852)	0.961(0.930–0.979)	0.896(0.809–0.944)
MUSE	0.830(0.706–0.954)	0.744(0.581–0.907)	0.906(0.830–0.950)	0.826(0.685–0.912)	0.735(0.510–0.856)	0.711(0.448–0.836)	0.974(0.952–0.986)	0.949(0.906–0.972)
FOCUS MUSE	0.771(0.578–0.964)	0.801(0.669–0.933)	0.776(0.592–0.881)	0.868(0.731–0.924)	0.799(0.627–0.891)	0.853(0.633–0.913)	0.964(0.934–0.981)	0.922(0.855–0.957)

Data was presented as mean (95 % confidence interval).
SS = single-shot diffusion-weighted imaging; FOCUS = field of view optimized and constrained undistorted single-shot diffusion-weighted imaging; MUSE DWI = multiplexed sensitivity encoding diffusion-weighted imaging; FOCUS MUSE = field of view optimized and constrained undistorted multiplexed sensitivity encoding diffusion-weighted imaging.

Table 3
Comparisons of subjective score, SNR, DR, and ADC among the four sequences by the Friedman test.

	SS	FOCUS SS	MUSE	FOCUS MUSE	P value
Subjective score	3.85 ± 0.65	4.01 ± 0.70	4.06 ± 0.66	4.58 ± 0.61	<0.001
SNR	52.97 ± 30.97	57.92 ± 33.84	72.23 ± 45.30	52.26 ± 35.94	<0.001
DR	0.68 ± 0.45	0.57 ± 0.35	0.60 ± 0.40	0.31 ± 0.22	<0.001
ADC ($\times 10^{-3}$ mm^2/s)	1.39 ± 0.43	1.38 ± 0.45	1.44 ± 0.49	1.34 ± 0.46	0.057

Note:Data were presented as mean ± standard derivation.
SNR = signal-to-noise ratio; DR = distortion ratio; ADC = apparent diffusion coefficient; SS = single-shot diffusion-weighted imaging; FOCUS = field of view optimized and constrained undistorted single-shot diffusion-weighted imaging; MUSE DWI = multiplexed sensitivity encoding diffusion-weighted imaging; FOCUS MUSE = field of view optimized and constrained undistorted multiplexed sensitivity encoding diffusion-weighted imaging.

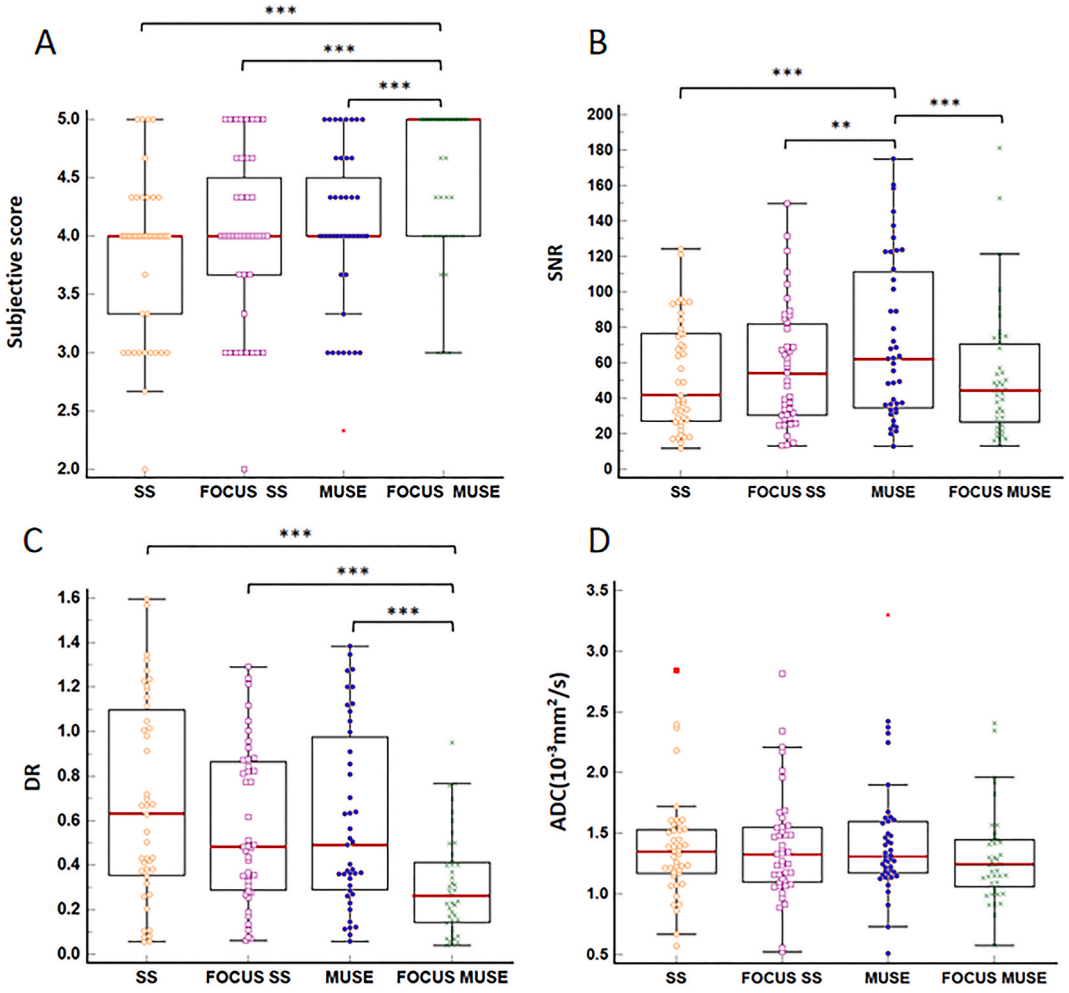

Fig. 1. Subjective score, SNR, DR, and ADC values of the four DWI sequences. *, P < 0.05; **, P < 0.01; ***, P < 0.001.

shown in Figs. 2–4 to visually depict the performance of the four sequences for delineating pulmonary lesion.

3.4. Comparisons of the performance of ADC for benign and malignant discrimination

As shown in Table 4, the ADC value of malignant was significantly smaller than that of benign with the P value of 0.022, 0.01, 0.036, and 0.002 for SS, FOCUS SS, MUSE, and FOCUS MUSE, respectively. The statistical power of all the four sequences for the ADC comparison between benign and malignant pulmonary lesions were greater than 0.85.

Fig. 5 showed the ROC results for distinguishing malignant from benign pulmonary lesions. All the four sequences can significantly differ benign and malignant lesions (P < 0.05). The FOCUS MUSE presented the best diagnostic performance with AUC of 0.820,

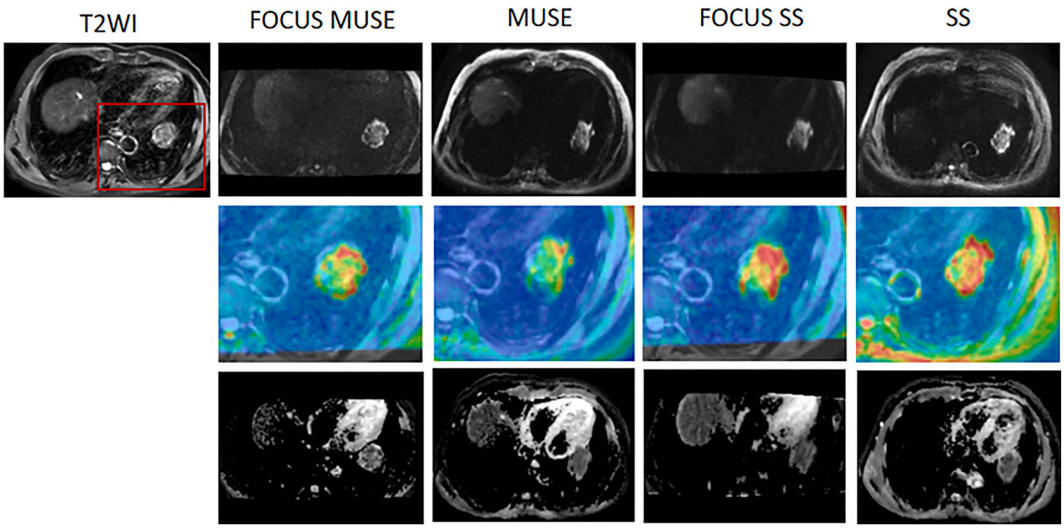

Fig. 2. Seventy-five years old man with nonidentified NSCLC in the left lower lobe. The diameter of tumor is about 4 cm. The first row was T2WI and location matched FOCUS MUSE, MUSE, FOCUS SS, and SS DWI images sequentially. The second row was corresponded and enlarged images with DWI overlayed on T2WI. The location of the enlarged region was shown in red rectangle on the T2WI image. The third row was the ADC map accordingly. Taking the anatomical T2WI as reference, the lesion was obviously stretched along the phase-encoding direction in SS. The same lesion was relatively less stretched in FOCUS SS and MUSE than in SS but shown susceptibility caused signal loss at the lesion-parenchyma interface. Among the four sequences, FOCUS MUSE showed the best image quality to delineate the round-shaped lesion which roughly matched in the anatomical T2WI. FOCUS MUSE as well as the derived ADC map also demonstrated best capability to characterize the heterogeneity organization of tumor. (For interpretation of the references to colour in this figure legend, the reader is referred to the Web version of this article.)

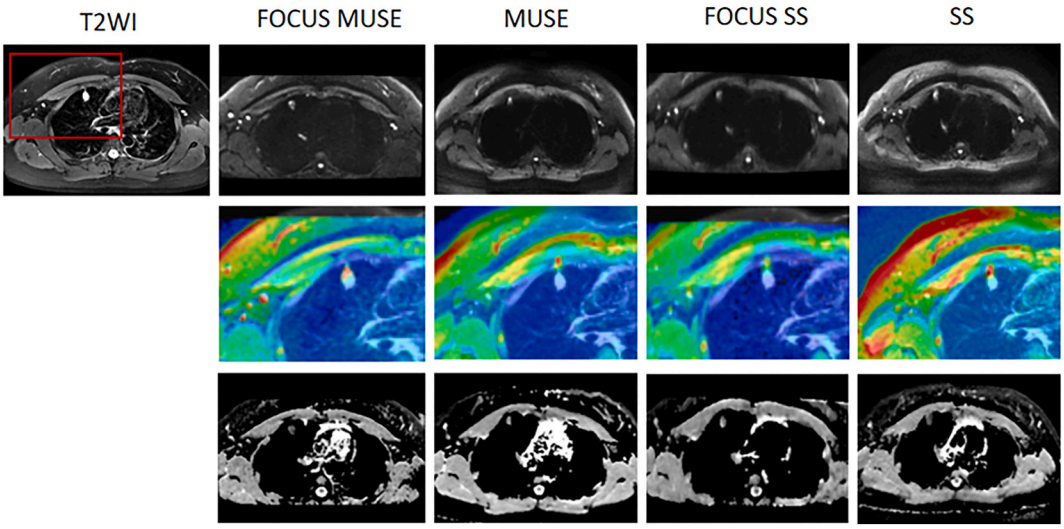

Fig. 3. Thirty-one years old woman with adenocarcinomas adjacent to chest wall in right lower lobe. The diameter of tumor is about 1.5 cm. The first row was T2WI and location matched FOCUS MUSE, MUSE, FOCUS SS, and SS DWI images sequentially. The second row was corresponded and enlarged images with DWI overlayed on T2WI. The location of the enlarged region was shown in red rectangle on the T2WI image. The third row was the ADC map accordingly. The overall shape and location of lesion were roughly compatible in FOCUS MUSE relative to T2WI. However, the same lesion was obviously distorted and spatial shifted on SS, FOCUS SS, and MUSE DWI images. (For interpretation of the references to colour in this figure legend, the reader is referred to the Web version of this article.)

sensitivity of 77.78 %, specificity of 73.53 %, and accuracy of 74.42 %, at the optimal threshold of 1.302 (10^{-3} mm^2/s). However, the diagnostic performance didn't show statistically different among the four sequences ($P > 0.05$).

4. Discussions

To the best of our knowledge, this was the first study investigating the value of improved EPI based DWI techniques, including

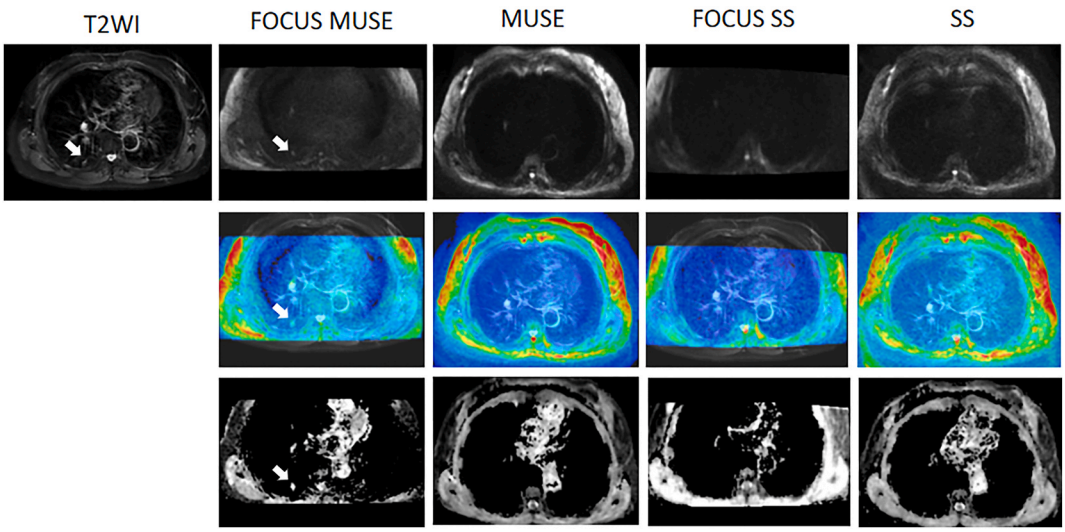

Fig. 4. Seventy-two years old woman with adenocarcinomas in the right upper lobe. The diameter of tumor is about 0.8 cm. The first row was T2WI and location matched FOCUS MUSE, MUSE, FOCUS SS, and SS DWI images sequentially. The second row was corresponded images with DWI overlayed on T2WI. The third row was the ADC map accordingly. The white arrows pointed the location of lesion. The lesion can be detected convincedly on FOCUS MUSE but not on SS, FOCUS SS, and MUSE.

Table 4
Comparison of ADC ($\times 10^{-3}$ mm^2/s) between benign and malignant lesions.

	SS	FOCUS SS	MUSE	FOCUS MUSE
Benign(n = 9)	1.82 ± 0.63	1.76 ± 0.53	1.88 ± 0.72	1.82 ± 0.66
Malignant(n = 34)	1.27 ± 0.28	1.28 ± 0.37	1.32 ± 0.33	1.21 ± 0.28
P value	0.022	0.01	0.036	0.002

Note:Data were presented as mean ± standard derivation.
SS = single-shot diffusion-weighted imaging; FOCUS = field of view optimized and constrained undistorted single-shot diffusion-weighted imaging; MUSE DWI = multiplexed sensitivity encoding diffusion-weighted imaging; FOCUS MUSE = field of view optimized and constrained undistorted multiplexed sensitivity encoding diffusion-weighted imaging.

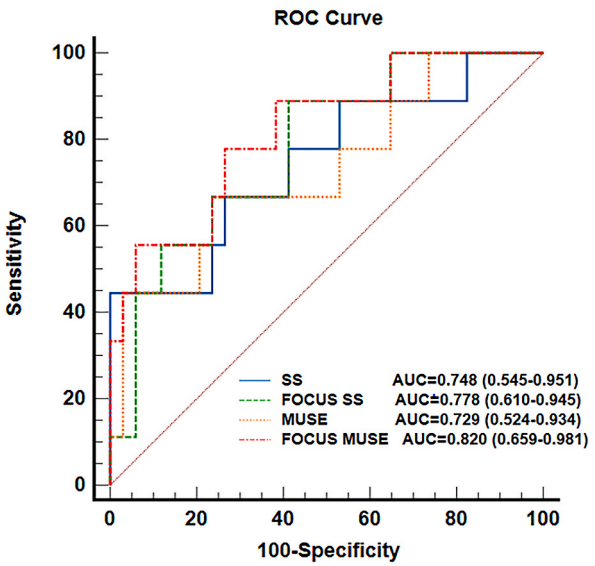

Fig. 5. The ROC curves of the four DWI sequences for distinguishing malignant from benign lesions.

FOCUS SS, MUSE, and FOCUS MUSE, for characterizing lung lesions. The results from our pilot study demonstrated FOCUS MUSE possessed sufficient SNR and significantly better image quality over routinely used SS as well as FOCUS SS, and MUSE, including significantly reduced distortion, better delineating and detecting of pulmonary lesions. FOCUS MUSE also showed relatively better diagnostic performance for distinguishing malignant from benign compared with other three DWI sequences. Therefore, the application of FOCUS MUSE would be beneficial for lung DWI. Due to CT is most widely used for pulmonary nodules detection and follow-up, for suspected malignant cases, direct surgery or biopsy may be chosen, so MRI may be suitable for cases with contraindications to surgery or biopsy. However, it should bear in mind that it's challenge for functional DWI to detect small pulmonary nodules (<10 mm).

DWI is a fundamental MRI technique in oncology and has emerging applications of lung. Abundant of quantitative microstructure information can be extracted from DWI and DWI based analytical/biophysical models, such as IVIM and DKI, which is important for tumor characterization and evaluation of treatment response and recurrence [6]. So far, a majority of lung DWI in clinic as well as in published studies have been carried out using SS-EPI technique for its fast imaging and decreased motion artifact properties [16]. However, the lung is an organ characterized by complex tissue-air interfaces leading to magnetic field inhomogeneities that make SS-EPI DWI prone to susceptibility artifacts and geometric distortion [6]. Using anatomical T2WI as reference, Tyagi et al. [20], Wan et al. [18], and Lei et al. [19], had reported pulmonary lesions were distorted and spatial shifted on SS-EPI DWI. Consistent results were also observed in our study (Figs. 2–3). Previous studies have shown FOCUS SS and MUSE DWI can reduce susceptibility related artifacts in other organs, including brain [29], thyroid gland [22], nasopharynx [23], pancreas [24], breast [25,31], rectum [26,30], columna vertebralis [27], cervix [32] and liver [33]. Nevertheless, our results didn't show similar results as expected. No significantly difference was found for the average/median value of overall image quality and DR among SS, FOCUS SS and MUSE (Table 3 and Fig. 1). The reason was likely because the tissue-air interfaces were too complex in lung to allow FOCUS SS and MUSE work well as in organs previously reported. In contrast, the image quality of FOCUS MUSE was significantly improved compared with routine SS-EPI as well as FOCUS SS and MUSE for lung DWI. Our results demonstrated the average/median subjective image score was significantly higher, and the DR was dramatically reduced for FOCUS MUSE in comparison with other three DWIs (Table 3 and Figs. 1–3). The shape and spatial location of lesion were roughly preserved in FOCUS MUSE relative to anatomical T2WI (Figs. 2–4). Similarly, Bai et al., reported FOCUS MUSE showed significantly better image quality of pancreatic than SS, FOCUS SS, and MUSE in term of overall image score and susceptibility artifacts [34]. The FOCUS MUSE had the best performance mainly because it inherits the advantages from both reduced FOV and segmented multi-shot imaging techniques [34].

FSE is also a fast acquisition technique and the application of FSE DWI goes far into last century [37]. Unlike SS-EPI DWI, FSE based acquisition is insensitive to main field inhomogeneities since the magnetic resonance signal can be refocused resulting with less susceptibility artifacts [9,20,37]. Thus, some researchers used FSE-based DWI for lung resulting with significant reduction of lesion distortion [18–20]. However, the scan time was much longer (more than three times), and the SNR was relatively or significantly lower for FSE DWI compared with SS-EPI DWI with the same image resolution [18,19]. In addition, the results of Lei et al., showed FSE DWI was relatively inferior to SS-EPI DWI in distinguishing malignant from benign pulmonary lesions [19]. FSE DWI was also bothered by the blurring of image [19]. In this study, our results showed FOCUS MUSE can also significantly reduce lung lesion distortion (Table 3 and Figs. 2–3). Compared FOCUS MUSE with SS-EPI DWI, our results showed the scan time was doubled (Table 1), the SNR was comparable (Table 3 and Fig. 1), more clear contrast of tumor heterogeneity (Fig. 2), and relatively superior to discriminate malignant from benign (Fig. 5). Similarly, Bai et al., found FOCUS MUSE provided sharper tissue contrast of pancreatic lesion than SS-EPI [34]. Although the scan time was doubled like in our study, the SNR of FOCUS MUSE was significantly higher than that of SS-EPI for pancreatic [34]. Hence, it seemed possible that the recently proposed FOCUS MUSE [34] was superior to FSE based technique for lung DWI in terms of scan time, SNR, tissue contrast, and the ability for benign and malignant discrimination. A comparison study between them should be further conducted.

Koyama et al. [38], and Regier et al. [39], had reported diagnostic potential of DWI in the detection of lung lesions. The DWI detection rate was 85 % for patients with lesion size range 5–69 mm in the study of Koyama et al., [38]. The results of Regier et al., showed only one lesion greater than 10 mm was missed at DWI because of a perception error of the readers [39]. However, the detection rate dropped to 86.4 % and 43.8 % for lesions with the size of 6–9 mm and 3–5 mm, respectively [39]. Consistent with the results of Regier et al., in our study, all the lesions with the diameter greater than 10 mm (n = 42) can be detected convincedly on all the four DWI images (Figs. 2–3). Only two patients with maximum lesion size of 6 mm and 8 mm were recruited in current study. Both lesions can be clearly inspected on FOCUS MUSE, and the overall shape and spatial location of them roughly matched to anatomical T2WI. However, on other three DWIs, the 6 mm lesion was distorted (data not shown) while the 8 mm lesion was undetectable (Fig. 4). In our pilot study, patients with maximum lesion size larger than 5 mm was recruited. Nevertheless, in a patient with maximum lesion size of 14 mm, we also found one 4 mm lesion on FOCUS MUSE but not on SS, FOCUS SS, and MUSE (data not shown). Our results suggested FOCUS MUSE may improve the detection sensitivity of small pulmonary lesions (<10 mm), which would be evaluated in the future to include more small lung nodules.

DWI signal depends largely on tissue micro-organization, such as cell membrane, cell size, cell density, extracellular space size, etc., that tend to be distinctive among different tumor types and between different states for the same tumor [6,9]. Thus, numerous studies have used ADC derived from DWI to quantitatively discriminate malignant from benign tumors and distinguish histopathological subtype [5–9]. A lot of studies had reported ADC can significantly distinguish malignant from benign pulmonary lesions [5,7,8]. Consistent with these reports, our results revealed ADC value of malignant was significantly lower than that of benign for all the four DWIs (Table 4). The diagnostic performance of SS (AUC = 0.748), FOCUS SS (AUC = 0.778), MUSE (AUC = 0.729), and FOCUS MUSE (AUC = 0.820) was compatible with previous reports (AUC range 0.770–0.931) [5,7,8]. FOCUS MUSE had a better performance over other three DWIs although it was not statistically significant. Uto et al. [40], and Gumustas et al. [36], also used ADC to discriminate malignant from benign with a similar sample size and constituent (most malignant patients were NSCLCs) as our study as well as the

studies mentioned above [36,40]. Their results showed malignant had relatively lower ADC than benign, but the difference was not significant. The diagnostic performance of ADC was 0.6 in the study of Uto et al., while Gumusta et al., didn't present the result. They attributed the uncertain of ADC for discriminating malignant from benign to that lung DWI is troublesome of SNR, cardiac and respiratory motion, and susceptibility artifacts [36,40]. The ADC value of tumor can be affected by the b value used for DWI [41]. Cakmak et al. [5], reported an AUC of 0.931 using b value of 600 s/mm^2 which was higher than the results of Rashed et al., (0.80), Zhu et al., (0.77), and ours (0.729–0.820) with b value of 800 s/mm^2 [7,8]. Thus, the uncertain performance of ADC reported by Uto et al., and Gumusta et al., was also likely to be affected by the higher b value (1000 s/mm^2) [36,40]. Nevertheless, further studies should be conducted to validate if ADC was reliable to distinguish malignant from benign pulmonary lesions with different b values in large cohort.

Some limitations should be noted in this study. First, the sample size of the pilot study was relatively small (n = 44), particularly for benign (n = 9). Thus, further study with large cohort should be conducted to validate if FOCUS MUSE was superior to the other three DWIs for discriminating malignant from benign pulmonary lesions. Second, our pilot study didn't involve the diagnostic performance of the four DWIs for distinguishing histopathological subtypes of malignant pulmonary lesions and characterizing the cellularity of specified malignant tumor due to the small sample size. It will be conducted in our further study when different malignant subtypes of patients were accumulated with larger sample group.

5. Conclusion

Our pilot study showed that FOCUS MUSE provided superior DWI image quality than SS, FOCUS SS, and MUSE for characterizing pulmonary lesions. The application of FOCUS MUSE DWI might be beneficial for evaluating lung disease with lesion size larger than 10 mm in clinic.

Ethics declarations

This study was reviewed and approved by [Medical Ethics Committee of Shanghai Changzheng Hospital], with the approval number: [2023SL028], ethics approval date: [June 16, 2023].

All participants/patients (or their proxies/legal guardians) provided informed consent to participate in the study.

All participants/patients (or their proxies/legal guardians) provided informed consent for the publication of their anonymised case details and images.

Consent for publication

Not applicable.

Date availability statement

The datasets generated during and/or analyzed during the current study are available from the corresponding author on reasonable request.

Funding

This work was supported by National Key R&D Program of China [2022YFC2010002, 2022YFC2010000]; the National Natural Science Foundation of China [82171926, 81930049, 81871321]; Medical imaging database construction program of National Health Commission [YXFSC2022JJSJ002]; the clinical Innovative Project of Shanghai Changzheng Hospital [2020YLCYJ-Y24]; the program of Science and Technology Commission of Shanghai Municipality [21DZ2202600].

CRediT authorship contribution statement

Jie Li: Writing – original draft, Visualization, Supervision, Software, Resources, Investigation, Formal analysis, Data curation. **Yi Xia:** Writing – review & editing, Visualization, Supervision, Resources, Project administration, Methodology, Investigation, Conceptualization. **JianKun Dai:** Writing – review & editing, Visualization, Validation, Supervision, Software, Methodology, Formal analysis. **GuangYuan Sun:** Resources, Data curation. **MeiLing Xu:** Resources, Project administration, Methodology, Data curation. **XiaoQing Lin:** Methodology, Investigation, Formal analysis, Data curation. **LingLing Gu:** Project administration, Methodology. **Jie Shi:** Validation, Supervision, Software, Methodology. **ShiYuan Liu:** Writing – review & editing, Visualization, Validation, Supervision, Software, Resources, Project administration, Methodology, Investigation, Funding acquisition, Formal analysis, Data curation, Conceptualization. **Li Fan:** Writing – review & editing, Visualization, Validation, Supervision, Software, Resources, Project administration, Methodology, Investigation, Funding acquisition, Formal analysis, Data curation, Conceptualization.

Declaration of competing interest

The authors declare that they have no known competing financial interests or personal relationships that could have appeared to

influence the work reported in this paper.

Appendix A. Supplementary data

Supplementary data to this article can be found online at https://doi.org/10.1016/j.heliyon.2024.e35203.

References

[1] H. Sung, J. Ferlay, R.L. Siegel, M. Laversanne, I. Soerjomataram, A. Jemal, F. Bray, Global cancer statistics 2020: GLOBOCAN estimates of incidence and mortality worldwide for 36 cancers in 185 countries, CA A Cancer J. Clin. 71 (3) (2021) 209–249, https://doi.org/10.3322/caac.21660.

[2] T. Fang, N. Meng, P. Feng, Z. Huang, Z. Li, F. Fu, J. Yuan, Y. Yang, H. Liu, N. Roberts, M. Wang, A comparative study of amide proton transfer weighted imaging and intravoxel incoherent motion MRI techniques versus (18) F-fdg PET to distinguish solitary pulmonary lesions and their subtypes, J. Magn. Reson. Imag. 55 (5) (2022) 1376–1390, https://doi.org/10.1002/jmri.27977.

[3] Y. Ohno, Y. Ozawa, H. Koyama, T. Yoshikawa, D. Takenaka, H. Nagata, T. Ueda, H. Ikeda, H. Toyama, State of the art MR imaging for lung cancer TNM stage evaluation, Cancers 15 (3) (2023), https://doi.org/10.3390/cancers15030950.

[4] M.L. Schiebler, G. Parraga, W.B. Gefter, B. Madore, K.S. Lee, Y. Ohno, H.U. Kauczor, H. Hatabu, Synopsis from expanding applications of pulmonary MRI in the clinical evaluation of lung disorders: fleischner society position paper, Chest 159 (2) (2021) 492–495, https://doi.org/10.1016/j.chest.2020.09.075.

[5] V. Cakmak, F. Ufuk, N. Karabulut, Diffusion-weighted MRI of pulmonary lesions: comparison of apparent diffusion coefficient and lesion-to-spinal cord signal intensity ratio in lesion characterization, J. Magn. Reson. Imag. 45 (3) (2017) 845–854, https://doi.org/10.1002/jmri.25426.

[6] J. Broncano, K. Steinbrecher, K.M. Marquis, C.A. Raptis, J. Royuela Del Val, I. Vollmer, S. Bhalla, A. Luna, Diffusion-weighted imaging of the chest: a primer for radiologists, Radiographics 43 (7) (2023) e220138, https://doi.org/10.1148/rg.220138.

[7] M. Mahdavi Rashed, S. Nekooei, M. Nouri, N. Borji, A. Khadembashi, Evaluation of DWI and ADC sequences' diagnostic values in benign and malignant pulmonary lesions, Turk Thorac J 21 (6) (2020) 390–396, https://doi.org/10.5152/TurkThoracJ.2020.19007.

[8] Q. Zhu, C. Ren, J.J. Xu, M.J. Li, H.S. Yuan, X.H. Wang, Whole-lesion histogram analysis of mono-exponential and bi-exponential diffusion-weighted imaging in differentiating lung cancer from benign pulmonary lesions using 3 T MRI, Clin. Radiol. 76 (11) (2021) 846–853, https://doi.org/10.1016/j.crad.2021.07.003.

[9] M. Matoba, H. Tonami, T. Kondou, H. Yokota, K. Higashi, H. Toga, T. Sakuma, Lung carcinoma: diffusion-weighted mr imaging–preliminary evaluation with apparent diffusion coefficient, Radiology 243 (2) (2007) 570–577, https://doi.org/10.1148/radiol.2432060131.

[10] M.L. Wang, H. Zhang, H.J. Yu, H. Tan, L.Z. Hu, H.J. Kong, W.J. Mao, J. Xiao, H.C. Shi, An initial study on the comparison of diagnostic performance of (18)F-FDG PET/MR and (18)F-FDG PET/CT for thoracic staging of non-small cell lung cancer: focus on pleural invasion, Rev. Española Med. Nucl. Imagen Mol. 42 (1) (2023) 16–23, https://doi.org/10.1016/j.remnie.2021.12.007.

[11] K. Liu, Z. Ma, L. Feng, Apparent diffusion coefficient as an effective index for the therapeutic efficiency of brain chemoradiotherapy for brain metastases from lung cancer, BMC Med. Imag. 18 (1) (2018) 30, https://doi.org/10.1186/s12880-018-0275-3.

[12] X. Bao, D. Bian, X. Yang, Z. Wang, M. Shang, G. Jiang, J. Shi, Multiparametric MRI for evaluation of pathological response to the neoadjuvant chemo-immunotherapy in resectable non-small-cell lung cancer, Eur. Radiol. (2023), https://doi.org/10.1007/s00330-023-09813-8.

[13] J. Liu, H. Lv, J. Dong, X. Ding, Z. Han, S. Yang, Z. Ba, Diffusion-weighted magnetic resonance imaging for early detection of chemotherapy resistance in non-small cell lung cancer, Med. Sci. Mon. Int. Med. J. Exp. Clin. Res. 25 (2019) 6264–6270, https://doi.org/10.12659/MSM.914236.

[14] G. Li, R. Huang, M. Zhu, M. Du, J. Zhu, Z. Sun, K. Liu, Y. Li, Native T1-mapping and diffusion-weighted imaging (DWI) can be used to identify lung cancer pathological types and their correlation with Ki-67 expression, J. Thorac. Dis. 14 (2) (2022) 443–454, https://doi.org/10.21037/jtd-22-77.

[15] D. Santucci, E. Faiella, A. Calabrese, B. Beomonte Zobel, A. Ascione, B. Cerbelli, G. Iannello, P. Soda, C. de Felice, On the additional information provided by 3T-MRI ADC in predicting tumor cellularity and microscopic behavior, Cancers 13 (20) (2021), https://doi.org/10.3390/cancers13205167.

[16] L. Filli, S. Ghafoor, D. Kenkel, W. Liu, E. Weiland, G. Andreisek, T. Frauenfelder, V.M. Runge, A. Boss, Simultaneous multi-slice readout-segmented echo planar imaging for accelerated diffusion-weighted imaging of the breast, Eur. J. Radiol. 85 (1) (2016) 274–278, https://doi.org/10.1016/j.ejrad.2015.10.009.

[17] F.L. Besson, B. Fernandez, S. Faure, O. Mercier, A. Seferian, E. Blanchet, X. Mignard, A. Chetouani, S. Bulifon, S. Mussot, F. Parent, F. Bouderraoui, D. Montani, D. Mitilian, E. Fadel, M.R. Ghigna-Bellinzoni, H. Cherkaoui, C. Comtat, V. Lebon, E. Durand, Diffusion-weighted imaging voxelwise-matched analyses of lung cancer at 3.0-T PET/MRI: reverse phase encoding approach for echo-planar imaging distortion correction, Radiology 295 (3) (2020) 692–700, https://doi.org/10.1148/radiol.2020192013.

[18] Q. Wan, Q. Lei, P. Wang, J. Hu, T. Zhang, D. Yu, X. Li, C. Liang, Intravoxel incoherent motion diffusion-weighted imaging of lung cancer: comparison between turbo spin-echo and echo-planar imaging, J. Comput. Assist. Tomogr. 44 (3) (2020) 334–340, https://doi.org/10.1097/RCT.0000000000001004.

[19] Q. Lei, Q. Wan, L. Liu, J. Hu, W. Zuo, J. Li, G. Jiang, X. Li, Values of apparent diffusion coefficient and lesion-to-spinal cord signal intensity in diagnosing solitary pulmonary lesions: turbo spin-echo versus echo-planar imaging diffusion-weighted imaging, BioMed Res. Int. 2021 (2021) 3345953, https://doi.org/10.1155/2021/3345953.

[20] N. Tyagi, M. Cloutier, K. Zakian, J.O. Deasy, M. Hunt, A. Rimner, Diffusion-weighted MRI of the lung at 3T evaluated using echo-planar-based and single-shot turbo spin-echo-based acquisition techniques for radiotherapy applications, J. Appl. Clin. Med. Phys. 20 (1) (2019) 284–292, https://doi.org/10.1002/acm2.12493.

[21] M. Tanabe, M. Higashi, T. Benkert, H. Imai, K. Miyoshi, F. Kameda, S. Ariyoshi, K. Ihara, K. Ito, Reduced field-of-view diffusion-weighted magnetic resonance imaging of the pancreas with tilted excitation plane: a preliminary study, J. Magn. Reson. Imag. 54 (3) (2021) 715–720, https://doi.org/10.1002/jmri.27590.

[22] Y.F. Wang, Y. Ren, C.F. Zhu, L. Qian, Q. Yang, W.M. Deng, L.Y. Zou, Z. Liu, D.H. Luo, Optimising diffusion-weighted imaging of the thyroid gland using dedicated surface coil, Clin. Radiol. 77 (11) (2022) e791–e798, https://doi.org/10.1016/j.crad.2022.07.011.

[23] T. Meng, H. Liu, J. Liu, F. Wang, C. Xie, L. Ke, H. He, The investigation of reduced field-of-view diffusion-weighted imaging (DWI) in patients with nasopharyngeal carcinoma: comparison with conventional DWI, Acta Radiol. 64 (6) (2023) 2118–2125, https://doi.org/10.1177/02841851231159389.

[24] F. Donati, C. Casini, R. Cervelli, R. Morganti, P. Boraschi, Diffusion-weighted MRI of solid pancreatic lesions: comparison between reduced field-of-view and large field-of-view sequences, Eur. J. Radiol. 143 (2021) 109936, https://doi.org/10.1016/j.ejrad.2021.109936.

[25] S. Fang, J. Zhu, Y. Wang, J. Zhou, G. Wang, W. Xu, W. Zhang, The value of whole-lesion histogram analysis based on field-of-view optimized and constrained undistorted single shot (FOCUS) DWI for predicting axillary lymph node status in early-stage breast cancer, BMC Med. Imag. 22 (1) (2022) 163, https://doi.org/10.1186/s12880-022-00891-6.

[26] Y. Cheng, H. Jiang, H. Wang, Q. Tang, T. Liu, Application of field-of-view optimized and constrained undistorted single shot (FOCUS) with intravoxel incoherent motion (IVIM) in 3T in locally advanced rectal cancer, Dis. Markers 2021 (2021) 5565902, https://doi.org/10.1155/2021/5565902.

[27] J. Cao, S. Gao, C. Zhang, Y. Zhang, W. Sun, L. Cui, Differentiating atypical hemangiomas and vertebral metastases: a field-of-view (FOV) and FOCUS intravoxel incoherent motion (IVIM) diffusion-weighted imaging (DWI) study, Eur. Spine J. 29 (12) (2020) 3187–3193, https://doi.org/10.1007/s00586-020-06632-z.

[28] N.K. Chen, A. Guidon, H.C. Chang, A.W. Song, A robust multi-shot scan strategy for high-resolution diffusion weighted MRI enabled by multiplexed sensitivity-encoding (MUSE), Neuroimage 72 (2013) 41–47, https://doi.org/10.1016/j.neuroimage.2013.01.038.

[29] J. Johansson, K. Lagerstrand, L. Ivarsson, P.A. Svensson, H. Hebelka, S.E. Maier, Brain diffusion MRI with multiplexed sensitivity encoding for reduced distortion in a pediatric patient population, Magn. Reson. Imaging 87 (2022) 97–103, https://doi.org/10.1016/j.mri.2022.01.003.

[30] M. El Homsi, D.D.B. Bates, Y. Mazaheri, R. Sosa, N. Gangai, I. Petkovska, Multiplexed sensitivity-encoding diffusion-weighted imaging (MUSE) in diffusion-weighted imaging for rectal MRI: a quantitative and qualitative analysis at multiple b-values, Abdom Radiol (NY) 48 (2) (2023) 448–457, https://doi.org/10.1007/s00261-022-03710-2.

[31] Y. Hu, D.M. Ikeda, S.M. Pittman, D. Samarawickrama, A. Guidon, J. Rosenberg, S.T. Chen, S. Okamoto, B.L. Daniel, B.A. Hargreaves, C.J. Moran, Multishot diffusion-weighted MRI of the breast with multiplexed sensitivity encoding (MUSE) and shot locally low-rank (Shot-LLR) reconstructions, J. Magn. Reson. Imag. 53 (3) (2021) 807–817, https://doi.org/10.1002/jmri.27383.

[32] T. Ota, T. Tsuboyama, H. Onishi, A. Nakamoto, H. Fukui, K. Yano, T. Honda, K. Kiso, M. Tatsumi, N. Tomiyama, Diagnostic accuracy of MRI for evaluating myometrial invasion in endometrial cancer: a comparison of MUSE-DWI, rFOV-DWI, and DCE-MRI, Radiol. Med. 128 (6) (2023) 629–643, https://doi.org/10.1007/s11547-023-01635-4.

[33] Y.Y. Kim, M.J. Kim, S.M. Gho, N. Seo, Comparison of multiplexed sensitivity encoding and single-shot echo-planar imaging for diffusion-weighted imaging of the liver, Eur. J. Radiol. 132 (2020) 109292, https://doi.org/10.1016/j.ejrad.2020.109292.

[34] Y. Bai, Y. Pei, W.V. Liu, W. Liu, S. Xie, X. Wang, L. Zhong, J. Chen, L. Zhang, I.B. Masokano, W. Li, MRI: evaluating the application of FOCUS-MUSE diffusion-weighted imaging in the pancreas in comparison with FOCUS, MUSE, and single-shot DWIs, J. Magn. Reson. Imag. 57 (4) (2023) 1156–1171, https://doi.org/10.1002/jmri.28382.

[35] Q. Yan, S. Yang, J. Shen, S. Lu, F. Shan, Y. Shi, 3T magnetic resonance for evaluation of adult pulmonary tuberculosis, Int. J. Infect. Dis. 93 (2020) 287–294, https://doi.org/10.1016/j.ijid.2020.02.006.

[36] S. Gumustas, N. Inan, G. Akansel, E. Ciftci, A. Demirci, S.K. Ozkara, Differentiation of malignant and benign lung lesions with diffusion-weighted MR imaging, Radiol. Oncol. 46 (2) (2012) 106–113, https://doi.org/10.2478/v10019-012-0021-3.

[37] K.O. Lovblad, P.M. Jakob, Q. Chen, A.E. Baird, G. Schlaug, S. Warach, R.R. Edelman, Turbo spin-echo diffusion-weighted MR of ischemic stroke, AJNR Am J Neuroradiol 19 (2) (1998) 201–208. ; discussion 209.

[38] H. Koyama, Y. Ohno, N. Aoyama, Y. Onishi, K. Matsumoto, M. Nogami, D. Takenaka, W. Nishio, C. Ohbayashi, K. Sugimura, Comparison of STIR turbo SE imaging and diffusion-weighted imaging of the lung: capability for detection and subtype classification of pulmonary adenocarcinomas, Eur. Radiol. 20 (4) (2010) 790–800, https://doi.org/10.1007/s00330-009-1615-z.

[39] M. Regier, D. Schwarz, F.O. Henes, M. Groth, H. Kooijman, P.G. Begemann, G. Adam, Diffusion-weighted MR-imaging for the detection of pulmonary nodules at 1.5 Tesla: intraindividual comparison with multidetector computed tomography, J Med Imaging Radiat Oncol 55 (3) (2011) 266–274, https://doi.org/10.1111/j.1754-9485.2011.02263.x.

[40] T. Uto, Y. Takehara, Y. Nakamura, T. Naito, D. Hashimoto, N. Inui, T. Suda, H. Nakamura, K. Chida, Higher sensitivity and specificity for diffusion-weighted imaging of malignant lung lesions without apparent diffusion coefficient quantification, Radiology 252 (1) (2009) 247–254, https://doi.org/10.1148/radiol.2521081195.

[41] M. Iima, S.C. Partridge, D. Le Bihan, Six DWI questions you always wanted to know but were afraid to ask: clinical relevance for breast diffusion MRI, Eur. Radiol. 30 (5) (2020) 2561–2570, https://doi.org/10.1007/s00330-019-06648-0.